Electronic Supplementary Material (ESI) for Dalton Transactions.
This journal is © The Royal Society of Chemistry 2022

Supporting Information

Carbon-incorporated bimetallic phosphides nanospheres derived from MOFs as superior electrocatalysts for hydrogen evolution

Xiaoxuan Shao,[a] Shusheng Xu,*[a] Peijie Wang,[a] Yi Wen,[a] Xuecheng Sun,*[b] Min Hong,[c] Kaiwei Wu[a] and Xue-Rong Shi*[a]

[a.] *School of Materials Engineering, Shanghai University of Engineering Science, Shanghai, 201620, P.R. China. E-mail: xushusheng@sues.edu.cn, E-mail: shixuer05@mails.ucas.ac.cn.*

[b.] *Microelectronic Research & Development Center, School of Mechatronics Engineering and Automation, Shanghai University, Shanghai, 200444, P. R. China. E-mail: sunxc@shu.edu.cn*

[c.] *Frontiers Science Center for Transformative Molecules, School of Chemistry and Chemical Engineering, Shanghai Jiao Tong University, Shanghai 200240, China*

Chemicals and Reagents

The chemicals we used in the experiment are of analytical grade (AR) and were directly used without any further purification. Polyvinylpyrrolidone (PVP), N, N-Dimethylformamide (DMF), Cobalt(II) acetylacetonate ($Co(acac)_2$), Iron(III) acetylacetonate ($Fe(acac)_3$) and ethanol were all purchased from Shanghai Titan Scientific Co. , Ltd. Sodium hypophosphite monohydrate ($NaH_2PO_2{\cdot}H_2O$) and 1,3,5-benzenetricarboxylic acid (H_3BTC) were obtained from Shanghai Aladdin Biochemical Technology. Ethylene glycol (EG) was obtained from Sinopharm Chemical Reagent Co. , Ltd.

Optimized H adsorption configuration.

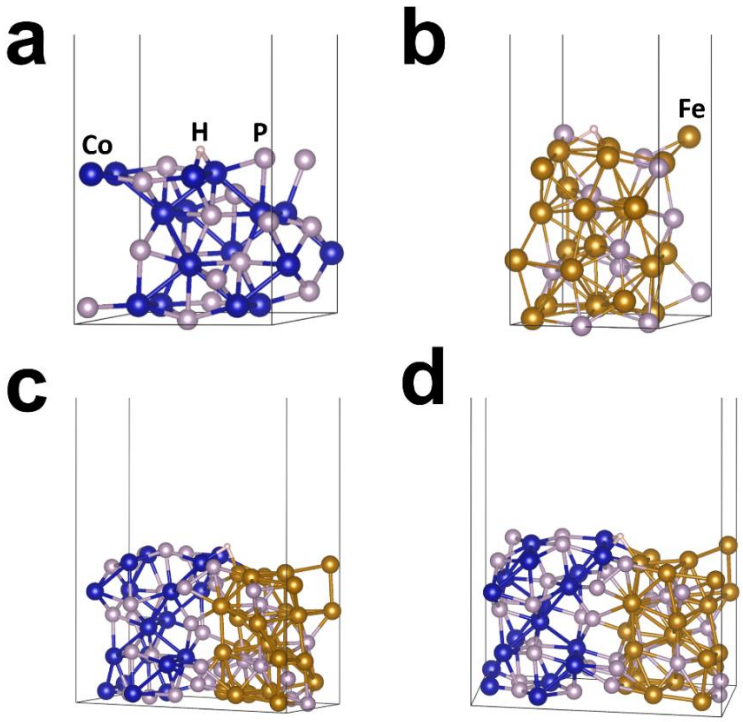

Fig. S1. Side views of the most favorable H adsorption configurations on (a) CoP(211), (b) Fe_2P(111), and (c, d) CoP(211)-Fe_2P(111): The black lines are the boundary lines of the unit-cell. 15 Å vacuum layer was added along z direction.

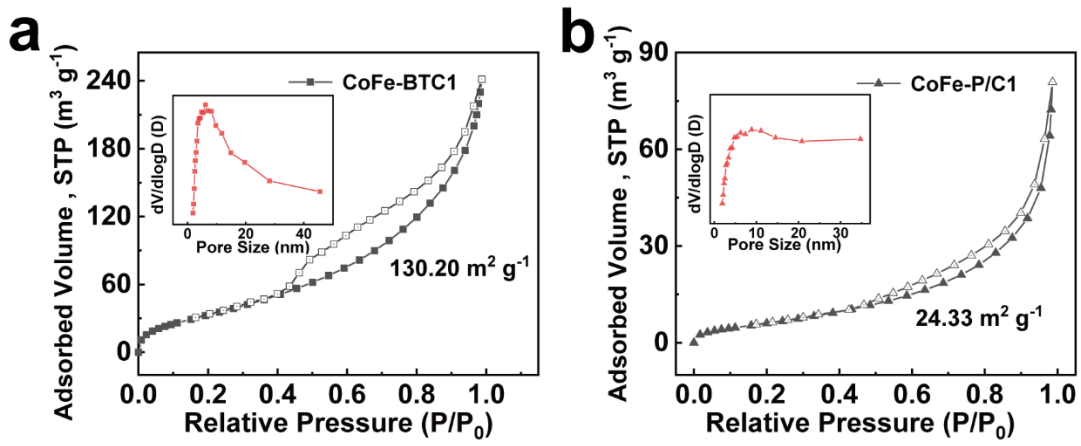

Fig. S2. The adsorption-desorption isotherms and pore size distribution profiles of (a) CoFe-BTC1 and (b) CoFe-P/C1.

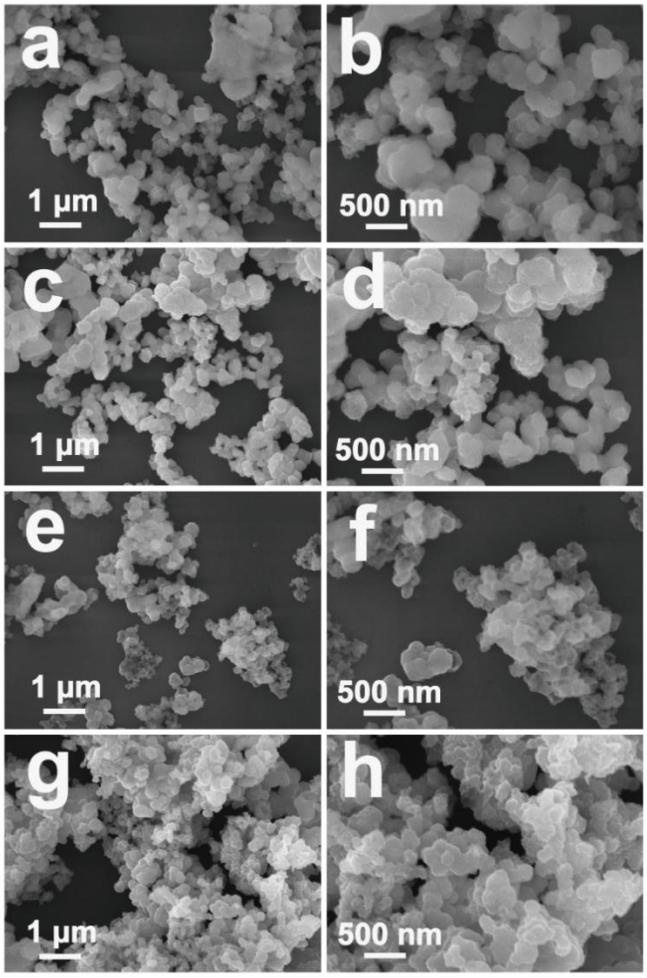

Fig. S3. The SEM images of (a, b) CoFe-BTC2, (c, d) CoFe-P/C2, (e, f) CoFe-BTC3, and (g, h) CoFe-P/C3.

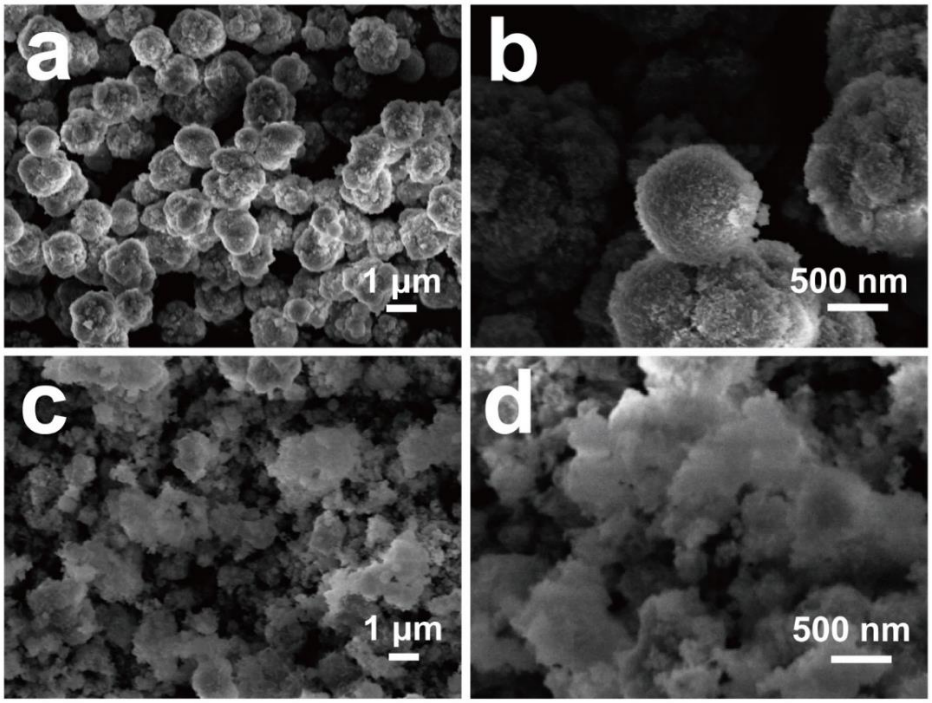

Fig. S4. SEM images of (a, b) CoP/C and (c, d) FeP/C.

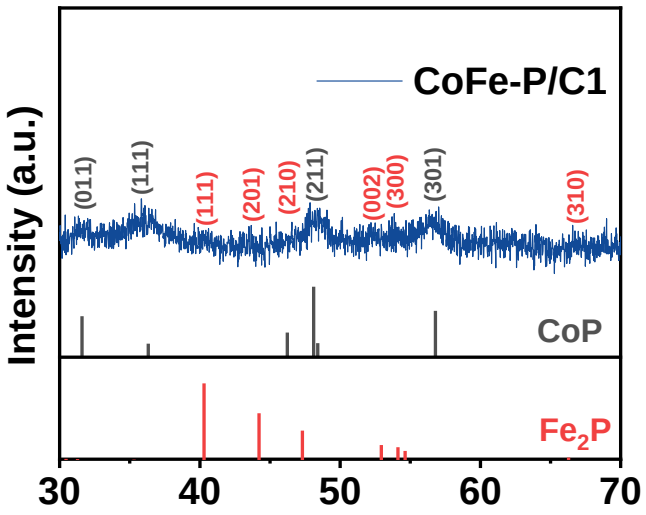

Fig. S5. The XRD spectra of CoFe-P/C1 at 30-70°

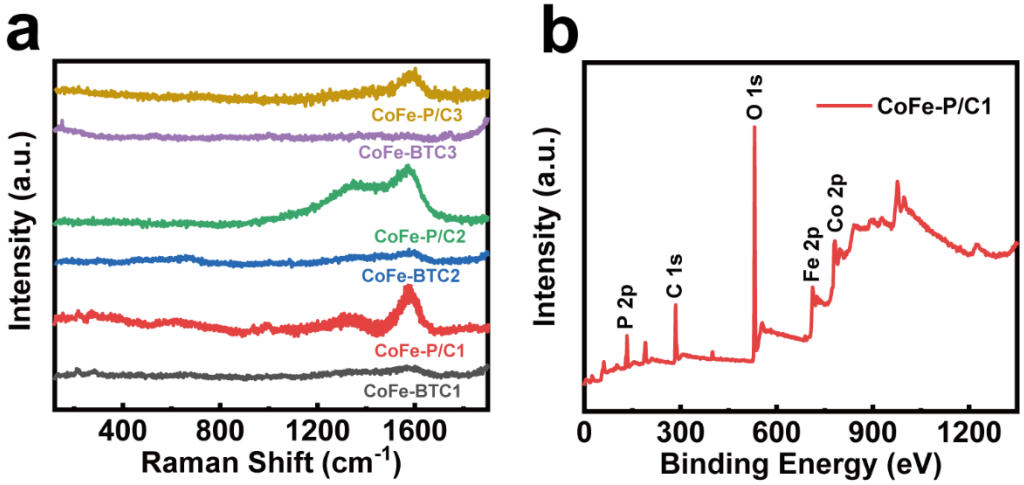

Fig. S6. (a) The Raman patterns of CoFe-BTC1, CoFe-P/C1, CoFe-BTC2, CoFe-P/C2, CoFe-BTC3, and CoFe-P/C3, (b) the XPS survey spectra of CoFe-P/C1.

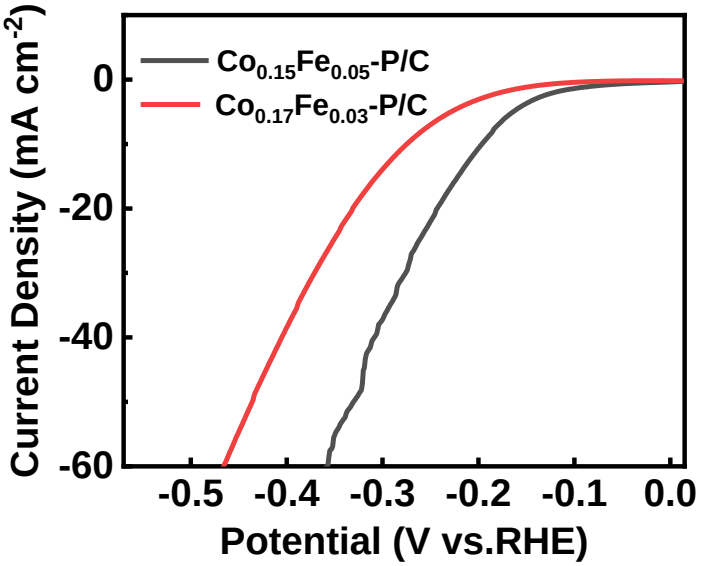

Fig. S7. LSV curves of the different Co:Fe ratios of 0.15:0.05 and 0.17:0.03.

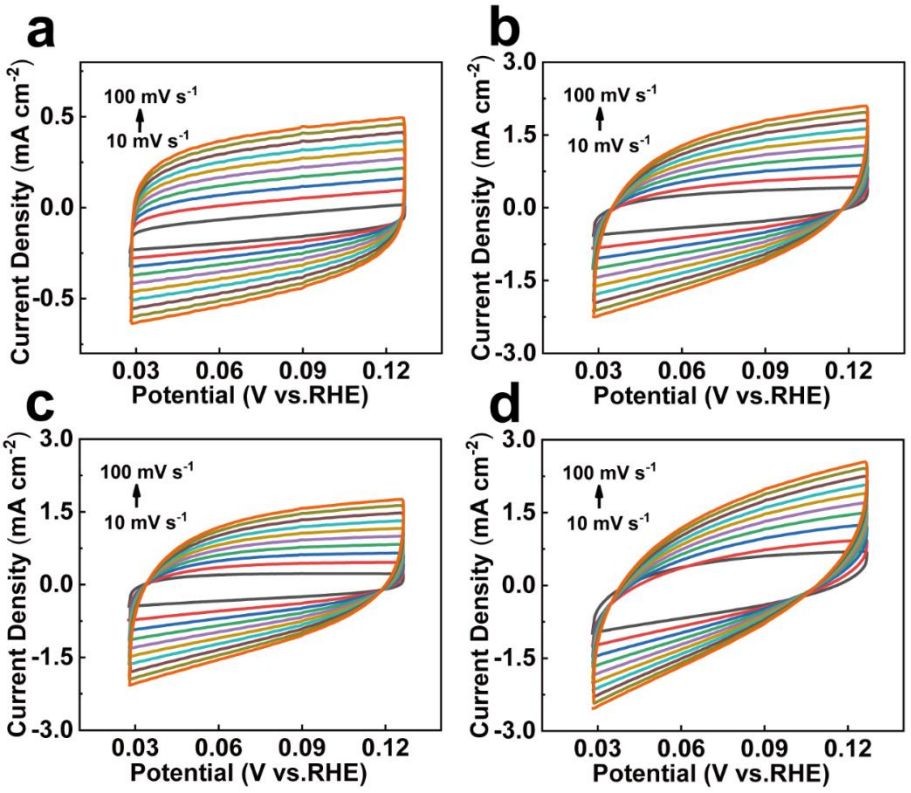

Fig. S8. The CV curves of (a) CoFe-BTC1, (b) CoFe-P/C1, (c) CoFe-P/C2, and (d) CoFe-P/C3 with various scan rates (10-100 mV s^{-1}) in the region of -1.0 to -0.9 V (vs. Ag/AgCl).

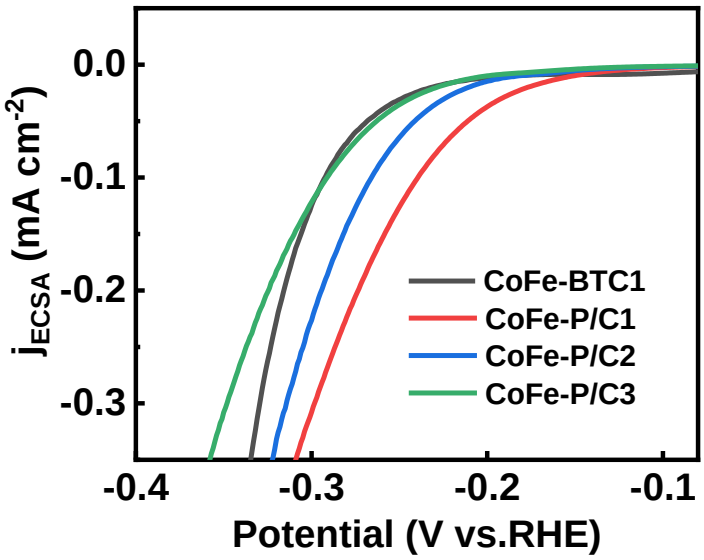

Fig. S9. ECSA-normalized LSV curves of CoFe-BTC1, CoFe-P/C1, CoFe-P/C2, and CoFe-P/C3 from **Fig. 3a**

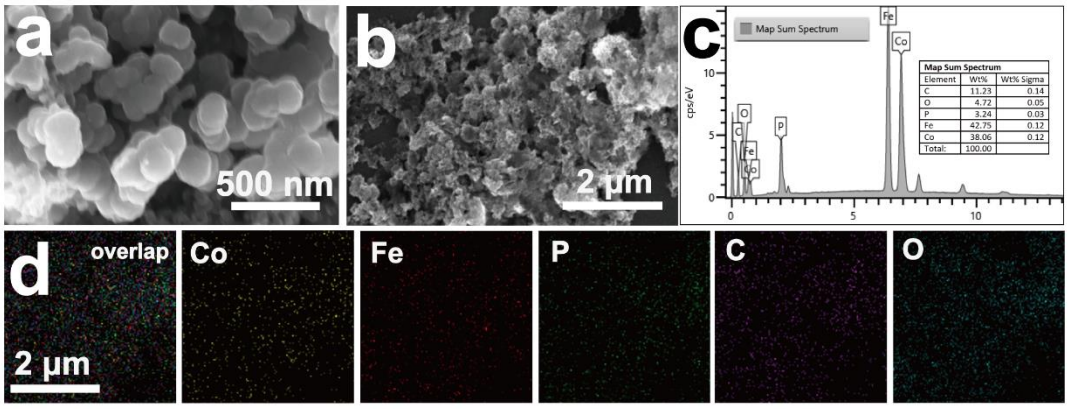

Fig. S10. (a, b) The SEM images, (c) EDS spectra, and (d) Elemental mapping images of CoFe-P/C1 after HER stability test in 1.0 M KOH solution for 12h.

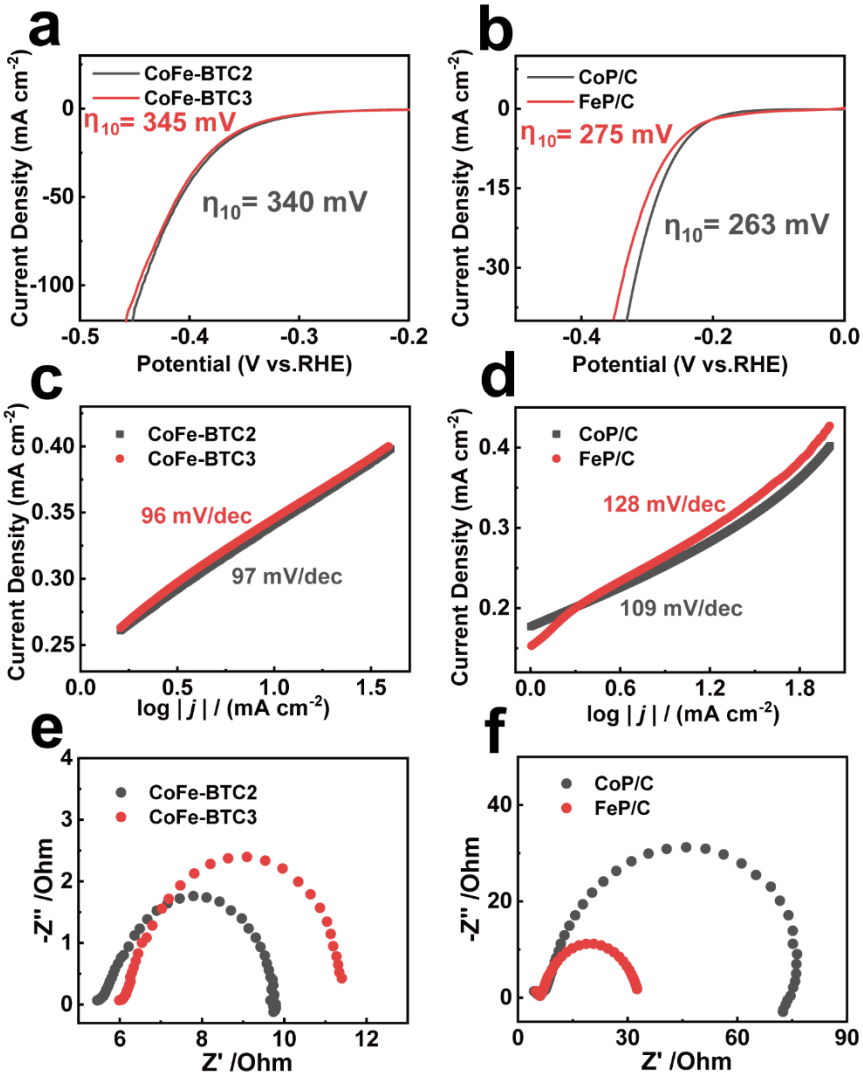

Fig. S11. The polarization curves of HER, Tafel slopes, and EIS curves in alkaline solution of (a, c, e) CoFe-BTC precursors with different Co/Fe ratios, and (b, d, f) the single metal phosphides (including CoP/C and FeP/C).

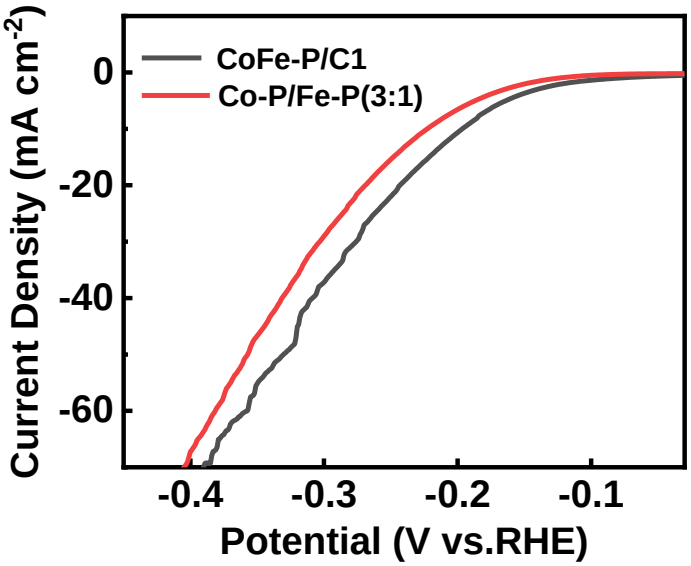

Fig. S12. LSV curves of CoFe-P/C1 and the physically mixed sample Co-P/Fe-P (3:1)

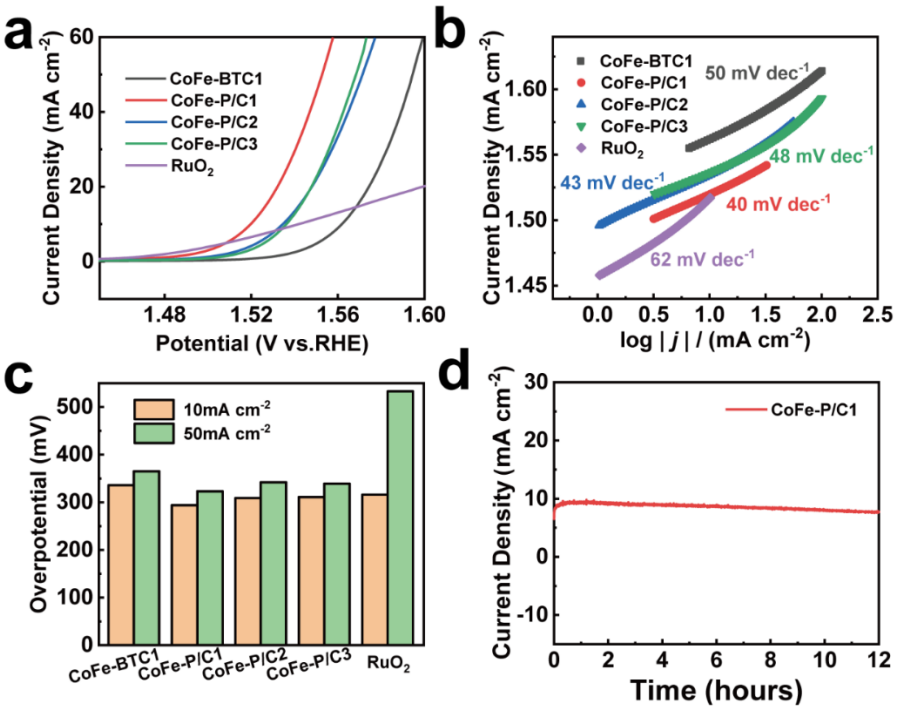

Fig. S13. (a) The polarization curves of OER, (b) the Tafel slopes corresponded, and (c) the listed overpotential data at 10 mA cm^{-2} of RuO_2, CoFe-P/C1, CoFe-P/C2, CoFe-P/C3, and CoFe-BTC1 in 1.0 M KOH. (d) The long-term stability test of CoFe-P/C1 at 0.494 V in alkaline solution.

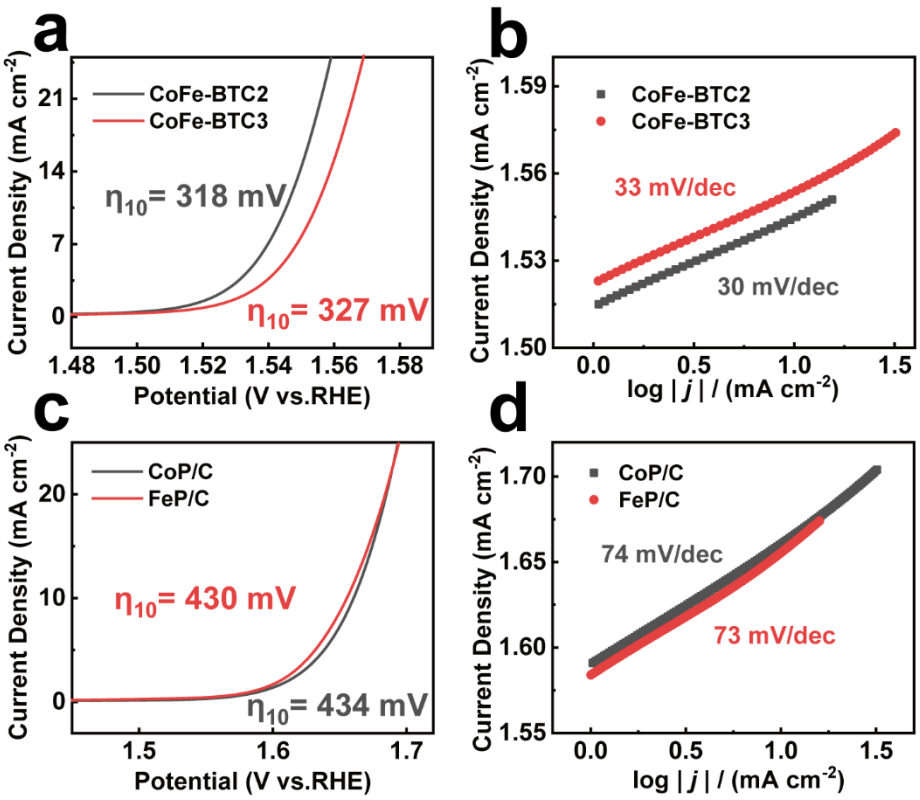

Fig. S14. The polarization curves of OER and Tafel slopes corresponded in alkaline solution of (a, b) CoFe-BTC precursors with different Co/Fe ratios and (c, d) the single metal phosphides (including CoP/C and FeP/C).

Table S1. Comparison of electrocatalytic performances of CoFe-P/C1 with other TMP-based electrocatalysts for HER in alkaline and acid solution.

Catalysts	Current Density (j)	Overpotential (η) at (j)	Tafel Slope	Electrolyte	Ref.
CoFe-P/C1	**10**	**193**	**78**	**1.0 M KOH**	**This work**
CoFe-P/C1	**10**	**138**	**84**	**0.5 M H_2SO_4**	**This work**
NiCoP/rGO	10	209	124	1.0 M KOH	[1]
Ni-Fe/NC	10	219	110	1.0 M KOH	[2]
CoFeP@NSOC-300	10	228	90	1.0 M KOH	[3]
CoFeP@NSOC-500	10	250	115	1.0 M KOH	[3]
NiFeP/NF	10	226.1	107	1.0 M KOH	[4]
NiFeP	10	243	69	1.0 M KOH	[5]
CoP NRAs	10	181	69	0.5 M H_2SO_4	[6]
Mn-CoP	10	148	61	0.5 M H_2SO_4	[7]

Table S2. Comparison of electrocatalytic performances of CoFe-P/C1 with other TMP-based electrocatalysts for OER in alkaline solution.

Catalysts	Current Density (j)	Overpotential (η) at (j)	Tafel Slope	Electrolyte	Ref.
CoFe-P/C1	**10**	**293**	**40**	**1.0 M KOH**	**This work**
CoNiP-1:1 NWs	10	301	54	1.0 M KOH	[8]
$Ni1Co_3$-P@CSs	10	330	113	1.0 M KOH	[9]
$NiCo_2S_4$ NWs	10	336	89	1.0 M KOH	[10]
FeNiP/NPCS	10	318	95	1.0 M KOH	[11]
NiCoP	10	336	109	1.0 M KOH	[12]
NiCoP/C	10	330	96	1.0 M KOH	[13]
Co-Ni-P film/Ti	10	340	67	1.0 M KOH	[14]
CoNiP/Ti	10	310	52	1.0 M KOH	[15]

Table S3. Comparison of electrocatalytic performances of CoFe-P/C1 with other TMP-based electrocatalysts for overall water splitting in alkaline solution.

Catalysts	Current Density (j)	Voltage (V)	Electrolyte	Ref.
CoFe-P/C1	**10**	**1.62**	**1.0 M KOH**	**This work**
FeCo@FeCoP@C@NCCs	10	1.64	1.0 M KOH	[16]
amorphous NiFeCoP/Ni mesh	10	1.64	1.0 M KOH	[9]
C-(Fe-Ni)P@PC/(Ni-Co)P@CC	10	1.63	1.0 M KOH	[17]
NiCoP-NSAs/NF	10	1.77	1.0 M KOH	[18]
NiCoP	10	1.65	1.0 M KOH	[14]
Co/NBC-900/GCE	10	1.68	1.0 M KOH	[19]
Co-Ni-P film/Ti	10	1.71	1.0 M KOH	[11]

References

1 J. Li, M. Yan, X. Zhou, Z. Q. Huang, Z. Xia, C. R. Chang, Y. Ma and Y. Qu, *Advanced Functional Materials*, 2016, **26**, 6785-6796.

2 X. Zhang, H. Xu, X. Li, Y. Li, T. Yang and Y. Liang, *ACS Catalysis*, 2016, **6**, 580-588.

3 Y. Zhang, L. Li, J. Chen, Y. Ma and X. Yang, *Ceramics International*, 2021, **47**, 12843-12850.

4 Y. Lin, M. Zhang, L. Zhao, L. Wang, D. Cao and Y. Gong, *Applied Surface Science*, 2021, **536**, 147952.

5 Y. Du, Z. Li, Y. Liu, Y. Yang and L. Wang, *Applied Surface Science*, 2018, **457**, 1081-1086.

6 L. Li, X. Li, L. Ai and J. Jiang, *RSC Advances*, 2015, **5**, 90265-90271.

7 Y. Li, B. Jia, B. Chen, Q. Liu, M. Cai, Z. Xue, Y. Fan, H. P. Wang, C. Y. Su and G. Li, *Dalton Transactions*, 2018, **47**, 14679-14685.

8 I. Amorim, J. Xu, N. Zhang, D. Xiong, S. M. Thalluri, R. Thomas, J. P. S. Sousa, A. Araújo, H. Li and L. Liu, *Catalysis Today*, 2020, **358**, 196-202.

9 V. H. Hoa, D. T. Tran, H. T. Le, N. H. Kim and J. H. Lee, *Applied Catalysis B: Environmental*, 2019, **253**, 235-245.

10 D. Liu, Q. Lu, Y. Luo, X. Sun and A. M. Asiri, *Nanoscale*, 2015, **7**, 15122-15126.

11 J. T. Ren, Y. S. Wang, L. Chen, L. J. Gao, W. W. Tian and Z. Y. Yuan, *Chemical Engineering Journal*, 2020, **389**, 124408.

12 R. Zhang, J. Huang, G. Chen, W. Chen, C. Song, C. Li and K. Ostrikov, *Applied Catalysis B: Environmental*, 2019, **254**, 414-423.

13 P. He, X. Y. Yu and X. W. D. Lou, *Angewandte Chemie - International Edition*, 2017, **56**, 3897-3900.

14 Y. Pei, Y. Yang, F. Zhang, P. Dong, R. Baines, Y. Ge, H. Chu, P. M. Ajayan, J. Shen and M. Ye, *ACS Applied Materials and Interfaces*, 2017, **9**, 31887-31896.

15 C. Wang, J. Jiang, T. Ding, G. Chen, W. Xu and Q. Yang, *Advanced Materials Interfaces*, **3**, 1500454.

16 Y. Li, S. Li, J. Hu, Y. Zhang, Y. Du, X. Han, X. Liu and P. Xu, *Journal of Energy Chemistry*, 2020, **53**, 1-8.

17 C. N. Lv, L. Zhang, X. H. Huang, Y. X. Zhu, X. Zhang, J. S. Hu and S. Y. Lu, *Nano Energy*, 2019, **65**, 103995.

18 Y. Li, H. Zhang, M. Jiang, Y. Kuang, X. Sun and X. Duan, *Nano Research*, 2016, **9**, 2251-2259.

19 M. R. Liu, Q. L. Hong, Q. H. Li, Y. Du, H. X. Zhang, S. Chen, T. Zhou and J. Zhang, *Advanced Functional Materials*, **28**, 1801136.